Monthly Notices of the ROYAL ASTRONOMICAL SOCIETY

MNRAS **526,** 3482–3494 (2023) https://doi.org/10.1093/mnras/stad2964
Advance Access publication 2023 September 28

# Optimized temporal binning of comparison star measurements for differential photometry

Kathryn E. Hartley ★ and R. W. Wilson

*Centre for Advanced Instrumentation, Department of Physics, University of Durham, South Road, Durham DH1 3LE, UK*

Accepted 2023 September 25. Received 2023 September 15; in original form 2023 March 20

## ABSTRACT

Ground-based, high precision observations of the light curves of objects such as transiting exoplanets rely on the application of differential photometry. The flux of the target object is measured relative to a comparison star in the same field, allowing correction for systematic trends in the light curve, mainly due to atmospheric effects including the variation of extinction with airmass. However, the precision of the light curve is then limited by the random noise for the measurements of both the target object and the comparison star. For time-resolved photometry using short exposure times of up to a few tens of seconds, the time-scale of the systematic variations due to atmospheric (or other) effects can be much longer than the cadence of the observations. In this case, the overall signal-to-noise ratio of the observation may be improved significantly by applying some temporal binning to the measurements of the comparison star, before comparison with the target object, without reducing the cadence of the overall light curve. In this paper, we will describe a data reduction pipeline for implementing this method which optimizes the number of frames to be binned for the comparison star, and we present example results for time-resolved photometric data. An example of applying the technique on an exoplanet transit light curve of WASP-166b is presented using four comparison stars of different magnitudes.

**Key words:** atmospheric effects – methods: data analysis – techniques: photometric.

## 1 INTRODUCTION

High-precision time-resolved photometry is central to the study of variability of astronomical objects. However, ground-based observations are limited by effects of the Earth's atmosphere, including scintillation, absorption, and scattering. These introduce random intensity variations that are correlated on a range of time-scales and with a range of angular correlations.

Differential photometry aims to correct these systematic errors due to atmospheric and instrumental effects (Howell 1992). This technique has been particularly important for the studies of exoplanet transits (Pont, Zucker & Queloz 2006), eclipsing binaries (Pluzhnik, 2005), and microlensing events (Giannini, et al. 2017).

For ground-based differential photometry, the comparison star should be close to the target star in order to maximize the correlation for systematic trends. However, it should also be bright in order to minimize shot noise (Mann, Gaidos & Aldering 2011). It is difficult to meet both these requirements simultaneously, especially for large telescopes where the field of view (FOV) is more likely to be limited.

Furthermore, differential photometry cannot normally be used to correct scintillation noise since the angular correlation of the intensity fluctuations is very small (Kornilov 2012). Hence, the probability of there being a bright comparison star within the iso-photometric angle is small – of the order of a few arcseconds.

Although the use of comparison stars can be effective at removing systematic trends, the random noise for the comparison star and target star (such as photon and scintillation noise), add in quadrature, thus increasing the random noise in the calibrated light curve (Koppelman 2005). For the brightest targets, the random noise will typically be dominated by scintillation noise and will be independent of the magnitude. If the comparison star is also scintillation limited, then the variance of the noise in the calibrated light curve will be increased by a factor of 2 (see Fig. 1). For fainter comparison stars, where photon noise dominates, the noise-to-signal ratio (NSR) of the calibrated light curve will be increased by a larger factor. This significantly limits the number of comparison stars that can be used to perform effective differential photometry.

We propose that, since in many cases the time-scale of the systematic variations due to the atmosphere will be much longer than the cadence of the observations (Young et al. 1991), the comparison star data can be temporally binned before applying the calibration to the target star. Therefore, the NSR of the calibrated light curve will be significantly improved. This method can be applied to any data set with cadences of up to a few tens of seconds recorded in good photometric conditions and allows the use of much fainter comparison stars without detriment. This is especially advantageous when observing with large telescopes which tend to have a limited FOV. In all cases, we assume that it is not possible to reduce the cadence of the observations of the science target.

For light curves affected by short periods of high frequency trends, e.g. due to intermittent cirrus clouds, the temporal binning

★ E-mail: kathryn.e.hartley@durham.ac.uk

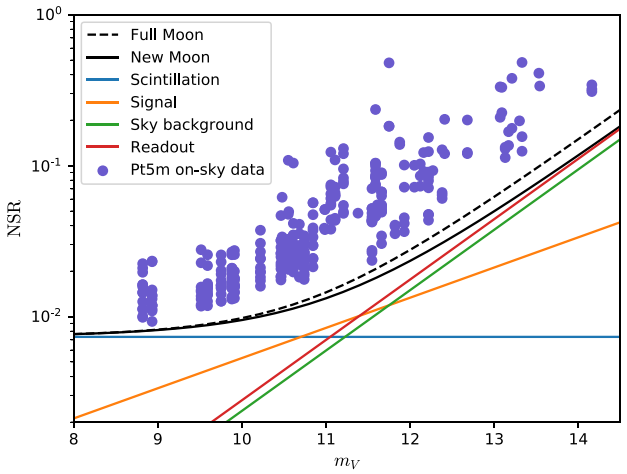


**Figure 1.** The measured NSR for light curves observed in the Pinwheel Cluster using the Pt5m telescope in the *V* band under typical atmospheric conditions for La Palma, Spain with an exposure time of 1 s are plotted (as blue data points) as a function of the stellar magnitude. The expected noise contributions from different sources including scintillation, signal noise, readout, and sky background are also plotted as a function of the star magnitude. The total noise is plotted for both full moon and new moon. The measured NSR for the light curves lie above the expected noise for the charged coupled device equation, as the light curves will also contain systematic noise.

can be applied everywhere apart from these periods. Hence, the improvement in NSR can still be achieved for a majority of the calibrated light curve.

In this paper, we describe a data reduction pipeline for implementing the method, which optimizes the number of frames to be temporally binned for the comparison star. We present some example results for time-resolved photometric data. Finally, we present results of applying this technique on an exoplanet transit light curve of WASP-166b (Doyle et al. 2022) and the results for a range of comparison star magnitudes are compared.

## 2 THEORY

### 2.1 Sources of photometric boise

#### *2.1.1 Charged coupled device (CCD) equation*

There are four main sources of photometric noise that are uncorrelated in both angle and time. These are:

(i) Photon noise – the shot noise of the signal from the source, which depends on its magnitude.

(ii) Sky background – shot noise of the background light from other sources (e.g. Moonlight).

(iii) Readout noise of the detector. This is a combination of noise in the conversion of charge into voltage and of noise in the amplification electronics that convert the signal from analogue to digital.

(iv) Dark current – shot noise of thermally induced electrons in the detector.

In the absence of correlated noise, the photometric SNR measured using a CCD detector is given by the CCD equation (Howell 1989):

$$\mathrm{SNR} = \frac{S_*}{\sqrt{S_* + n_{\mathrm{pix}}(\sigma_r^2 + B + D)}}, \tag{1}$$

where $S_*$ is the signal from the source, $n_{\mathrm{pix}}$ is the number of pixels in the photometric aperture used to sample the source, $\sigma_{\mathrm{r}}$ is the readout noise, $B$ is the sky background signal, and $D$ is the detector dark current. The NSR is given by 1/SNR.

Fig. 1 shows the relative noise contributions to the NSR as a function of the stellar magnitude. The plot was made for the Pt5m telescope (Hardy et al. 2015), a 50-cm aperture, in the *V* band assuming typical atmospheric conditions for La Palma, Spain with an exposure time of 1 s. Scintillation noise is dominant for bright stars below $V \approx 10$. For longer exposure times, the photon noise often becomes dominant for $V \approx 10$–15 after which the signal often becomes limited by sky background. In most cases, for long exposure times, readout and dark current are negligible.

Data from observations of the Pinwheel cluster from the Pt5m collected between December 2020 and April 2021 is plotted (see Section 5.1.1). These points lie above the expected noise for the CCD equation, as the light curves will also contain systematic noise.

#### *2.1.2 Scintillation*

Scintillation is the fluctuation of intensity produced by high altitude turbulence in the atmosphere. The mixing of layers of varying temperatures in the atmosphere results in spatially and temporally varying refractive indices. As the incoming wavefront passes through these high altitude turbulent layers, the wavefront is locally focused and de-focused resulting in spatial intensity fluctuations in the pupil plane of the telescope known as scintillation patterns (Osborn 2014). These patterns change with time as the turbulence moves with the wind and as it evolves (Dravins et al. 1997). For bright stars, this is the limiting noise source for photometry (Föhring et al. 2015).

For long exposure times, where the exposure time is longer than the time taken for the turbulent layer to cross the telescope pupil, the scintillation index is given by (Sasiela 2012)

$$\sigma_I^2 = 10.66 D^{-4/3} t^{-1} (\cos(\gamma))^{\alpha} \int_0^{\infty} \frac{h^2 C_n^2(h)}{V_{\perp}(h)} \mathrm{d}h, \tag{2}$$

where $t$ is the exposure time used, $D$ is the telescope aperture diameter, $h$ is the altitude of the turbulent layer, $C_n^2(h)$ is the refractive index structure constant (a measure of the vertical profile of the turbulence strength), $\gamma$ is the zenith angle, $\alpha$ is the exponent of the airmass, and $V_{\perp}(h)$ is the wind velocity profile. The value of $\alpha$ depends on the wind direction and will be $-3$ when the wind is transverse to the azimuthal angle of the star and $-4$ when it is longitudinal.

From equation (2), the scintillation noise reduces with the exposure time used. All ground-based optical light curve observations will be subject to scintillation noise. Currently, no scintillation correction techniques are in regular use-; however, a method that uses tomographic wavefront sensing has been proposed by Osborn (2014) and has been demonstrated on-sky (Hartley et al. 2023).

Since the angle over which the intensity fluctuations are correlated is only a few arcseconds, it cannot normally be corrected directly through differential photometry. This is because the probability of finding a bright comparison star within the iso-photometric angle is very small.

#### *2.1.3 Short-term atmospheric transparency variations*

As starlight passes through the Earth's atmosphere, molecular absorption and scattering from molecules and aerosols attenuate the incoming light (Zou et al. 2010). Such transparency variations have

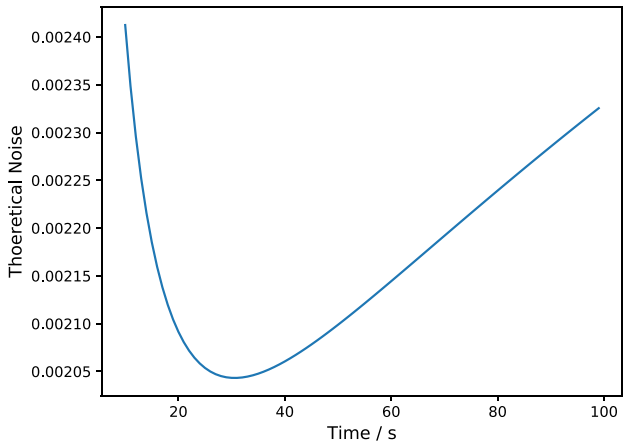


**Figure 2.** The theoretical noise as a function of the exposure time used. The plot was calculated assuming a star of magnitude 10 in the *V* band observed using the Pt5m telescope in standard atmospheric conditions for La Palma, Spain. We assumed that the systematic noise was due only to atmospheric transparency variations described by equation (3).

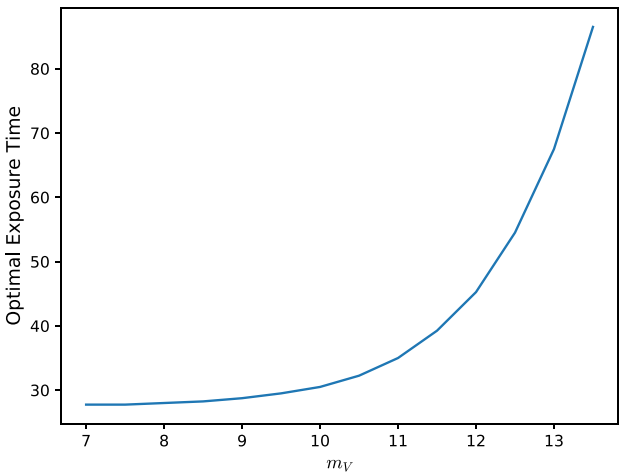


**Figure 3.** The optimal exposure time as a function of star magnitude. The plot was simulated assuming the stars were observed using the Pt5m telescope in standard atmospheric conditions for La Palma, Spain. We assumed that the systematic noise was due only to atmospheric transparency variations described by equation (3).

a power spectrum proportional to $1/f$ (Young et al. 1991) where $f$ is the temporal frequency.

From Hill et al. (1994), the average atmospheric transparency variations have a power spectrum given by

$$\log(P(\nu)) = -8.59 - 1.19\log(f). \quad (3)$$

Here, the coefficients were determined empirically from observations at the Observatorio del Teide, Tenerife. It should be noted that the measurements of this power spectrum were taken during the day for solar studies. It is unclear if the transparency variations would have the same power at night since aerosol inhomogeneities are much weaker (Young et al. 1991), but we assume that it will follow the same linear relationship with the log frequency.

Whilst on average the power spectrum of the transparency variations follow equation (3), on a given night the atmospheric transparency variations could be significantly higher or lower. In addition, the measured transparency can also vary seasonally (Zou et al. 2010). There is also strong dependence of the transmission on wavelength. Following Mann et al. (2011), we assume that a scaling factor can be applied to equation (3) to estimate the power spectrum for the waveband used.

#### *2.1.4 Other photometric errors*

Light curves also contain other sources of systematic noise, or 'red' noise. Systematic noise is always present in aperture photometry at some level. These systematic trends are due to atmospheric effects such as changes in airmass, systematics in the instrumentation such as telescope tracking and also systematic noise induced in the data reduction process such as flat-field errors. The process of performing the differential photometry also induces some small scale systematic noise due to first-order and second-order extinction effects. These are discussed in more detail in Section 2.3.

### 2.2 Total noise

The total noise in the light curve depends on the exposure time. From equations (1) and (2), the scintillation and photon noise will decrease with the exposure time. On the other hand, the noise due to the atmospheric transparency variations will increase with exposure time and hence the cadence of the light curve (Mann et al. 2011), as shown by equation (3). Therefore, for a given observation, there will be an optimal exposure time that minimizes the total noise. Fig. 2 shows an example of the theoretical photometric noise as a function of the exposure time.

The plot was calculated assuming a star of magnitude 10 in the *V* band observed using the Pt5m telescope. We assumed that the systematic noise was due only to atmospheric transparency variations described by equation (3).

The minimum in Fig. 2, only exists because of systematic trends in the light curve. Without such effects, the noise would continue to decrease with exposure time as the scintillation and shot noise decrease. Therefore, measuring the noise as a function of the exposure time can give information on the atmospheric transparency fluctuations at the telescope site.

This optimal exposure time will also vary depending on the magnitude of the star, with fainter stars having a longer optimal exposure time, as shown in Fig. 3. This is because for fainter stars, photon noise becomes more dominant.

### 2.3 Differential photometry

Differential photometry is a technique that has been used for over a century (Stebbins 1910) to correct for these extrinsic variations in magnitude (Howell & Jacoby 1986). The premise is to measure the difference in brightness of an astronomical source when compared with one or more non-varying reference sources.

For CCD arrays, the reference stars, also known as comparison stars, are often observed simultaneously in the same image frame such that the object of interest can be compared with the reference star. This allows correction of any atmospheric effects that change with time. From this, any inherent changes in magnitude of the astronomical source can be determined. When properly applied, differential photometry techniques can obtain high accuracies, with errors as low as $\pm 0.001$ magnitude (Howell 2006; Southworth et al. 2009).

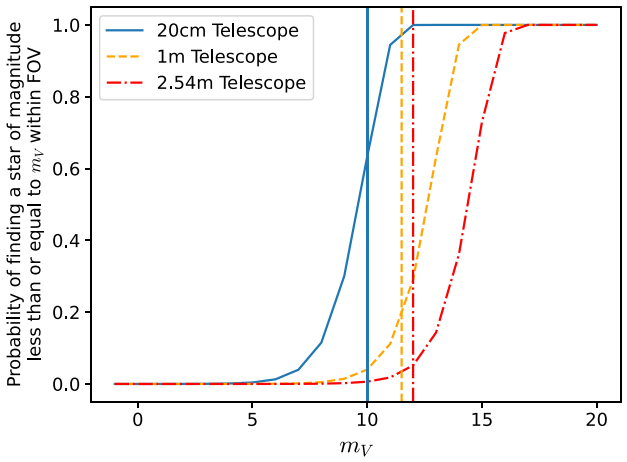


**Figure 4.** The average probability of finding a $V \leq m_V$ star within the FOV for a 20-cm, 1-m, and 2.54-m telescope. The vertical lines correspond to an estimate for the magnitude below which the photometric noise is dominated by scintillation.

Whilst using differential photometry does correct systematic trends in the target light curve, the process itself can also induce some small scale systematic effects such as first-order and second-order atmospheric extinction.

First-order atmospheric extinction is caused by the non-negligible difference in airmass between the target and comparison star. For long observations, lasting several hours, the differential airmass will change significantly (Mann et al. 2011). This results in the addition of a systematic trend to the calibrated light curve. As such, to minimize this systematic noise source, comparison stars close to the target of interest should be chosen.

Second-order extinction can also add systematic trends due to the difference in the spectral energy distribution over the pass-band, $\Delta\lambda$, between the target star and comparison star (Young et al. 1991). This effect is proportional to $\Delta\lambda^2$, and depends on the reddening of the Earth's atmosphere. As such, it changes from night to night. This effect can be minimized by selecting comparison stars close in colour to the target star.

In addition, comparison stars can only be used to correct systematic trends that are correlated with the target star. Flat fields can be used to correct field-dependent anomalies in the telescope optics and reduce effects of vignetting and pixel-to-pixel sensitivity variations. Ensuring that the target image is always centred on the same pixels can reduce instrumental systematic trends.

### 2.4 Sky coverage

As discussed in Section 2.3, the ideal comparison star should be close in the field to the target star and of a similar colour. Ideally, the star should be bright so as to minimize the addition of shot noise to the calibrated light curve.

The FOV of a telescope depends on the focal length and the physical size of the detector. For fixed values of the focal ratio, the FOV will scale inversely with the aperture size. Since most telescopes are produced for a range of fixed focal ratio values, larger telescopes will often have a smaller FOV.

Fig. 4 shows the average probability of finding a star of magnitude less than or equal to $m_V$ within the FOV for a 20 cm, 1 m, and 2.54 m telescopes for a fixed *f*-ratio of 10, and a ZWO ASI1600 detector. The vertical lines represent an estimate for the magnitude below which the photometric noise in a star light curve will be dominated by scintillation noise. For the two larger telescopes, where the FOV is smaller, the probability of there being a bright star is small. For the 20-cm telescope, there is a significantly higher probability of finding bright stars within its FOV. We note that this is the average probability across the whole sky.

The ideal comparison star would need to be as close as possible to the target star in order to minimize first-order extinction effects. Furthermore, ideally the comparison star should not be too near the edge of the detector to avoid the star drifting out of the frame over the observing period and to avoid vignetting effects. Therefore, the true probability of finding a suitable bright comparison star within the field is even more limited.

### 2.5 Temporal binning of comparison stars

Comparison stars are vital for high precision photometry. However, the calibrated light curve, although corrected for systematic noise, will now have increased random noise. This is because the NSR of the target star and of the comparison star add in quadrature.

Several advanced systematic correction techniques have previously been proposed and used. This includes the averaging of multiple comparison stars (Boyd 2007), therefore averaging the random fluctuations. However, as telescope aperture increases, the FOV decreases, thus reducing the likelihood of finding multiple suitable comparison stars to choose from.

Other techniques use curve fitting algorithms that measure low frequency trends in the comparison star light curve to remove low order trends in the data (Poddaný, Brát & Pejcha 2010). Whilst this method will not add any random noise, the technique makes assumptions about the order of the systematic noise and could miss periods of high frequency noise. The Kepler mission identifies systematic noise terms by searching for photometric trends common to a large ensemble of stars, specifically looking for trends with transit-length time-scales (Petigura & Marcy 2012).

We propose a new technique that takes advantage of the reduction in photon and scintillation noise with integration time. Since the systematic trends tend to be low in frequency, the comparison star signal can be binned in time with a moving average such that its noise is minimized. An integration time that minimizes the noise in the comparison star light curve exists, an example of this is shown in Fig. 2. Temporally binning the signal by this optimal factor reduces the random noise in the comparison star's light curve whilst retaining the low frequency trends. The temporally binned comparison star's light curve can then be used to normalize the photometry of the star of interest, thus correcting the systematic trends, whilst minimizing the addition of random noise.

Temporal binning is a technique widely used in astronomical photometry (Doyle et al. 2022) to reduce the NSR; however, it has traditionally been applied to the calibrated light curve as a whole. It should be noted that in our proposal, the light curve of the scientific target is not temporally binned and hence its cadence is unchanged. Only the comparison star signal is temporally binned. Our aim is that the NSR of the final calibrated light curve should be limited only by the random noise of the target star signal.

The comparison star is temporally binned with a moving average such that it has the same number of data points as the target signal. Using a moving average does introduce wings at the start and end of the light curve where the data cannot be averaged by $N_{\rm Bins}$ frames. However, in most applications, the period of interest will still have an improved NSR. Hence, when using this method one should ensure

that there are additional frames at the start and end of the observation run such that the period of interest is well covered.

For situations where both the target star and comparison star are bright and where scintillation noise is dominant, the NSR of the calibrated light curve can be reduced by a factor of up to $\sqrt{2}$, since they contribute equal noise variance. For fainter comparison stars where there is additional photon noise, the NSR of the calibrated target light curve can be reduced by up to $\sqrt{N_{\rm Bins}}$ where $N_{\rm Bins}$ is the number of frames which have been temporally binned for the comparison star. The optimum temporal binning for a given observation, an example of which is shown in Fig. 2, will depend on the magnitude of the comparison star used and on the power spectral density (PSD) of the systematic trends in the light curve.

The systematic trends in the light curve are not caused by the atmospheric transparency alone, there is additional systematic noise produced by the instrumentation optics and detectors. The atmospheric transparency variations and scintillation noise can also vary significantly from night to night. Therefore, it is very challenging to determine a theoretical value for the optimal degree of temporal binning.

The optimal degree of temporal binning to apply to the comparison star light curve is determined by finding the temporal binning factor that minimizes the NSR of the calibrated target light curve. However, since the target of interest will likely have intrinsic variation in its magnitude, a different non-varying star must be used to determine the optimal temporal binning factor. A pipeline to determine the optimal binning required for a given observation was developed and is detailed in Section 3.2.

For this technique, we assume that the observations are taken in good photometric conditions. It is assumed that the photometry does not contain high frequency systematic trends for example due to cirrus clouds, and that the primary source of systematic noise is due to atmospheric transparency variations. This technique cannot be applied for sources with blending.

This technique can be applied to either aperture photometry or PSF-fitting since the trade-off and optimization between the shot/scintillation noise and the systematic noise due to atmospheric transparency variations will still be the same. Hence, this technique can be applied to either case. In the examples in this paper, we only present aperture photometry.

## 3 METHOD

### 3.1 Quantifying systematic noise

The amount of systematic noise in the light curves can be estimated by a method known as RMS binning (Pont et al. 2006). The systematic noise is measured by splitting the signal up into $N$ bins and calculating the average standard deviation of the signal within each bin Fohring et al. (2013). For random white noise the standard deviation is proportional to the square root of the number of bins, $\sigma \propto 1/\sqrt{N}$.

In the presence of systematic noise, the gradient will deviate from that expected for pure white noise gradient. Hence, measuring the gradient indicates the amount of systematic noise in the light curve. This technique can also be used to visually determine whether the use of a comparison star has significantly reduced the systematic noise in the calibrated light curve. Plotting the root-mean-square (RMS) binning of the un-calibrated target light curve alongside the calibrated target light curve can be used to test whether using differential photometry has reduced the systematic noise for the target.

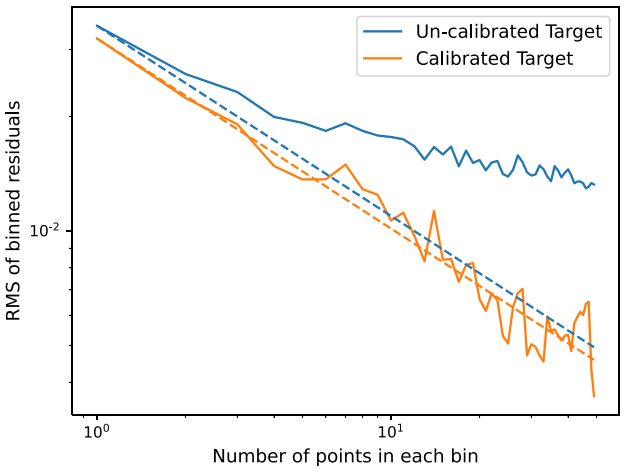


**Figure 5.** An example of the light curve RMS residual as a function of the number of points in each bin for the un-calibrated and calibrated light curve for an $m_V = 8.2$ star using an $m_V = 9.9$ comparison star in the Pinwheel cluster observed on the 2021 December 20 using the Pt5m telescope. The dashed lines show the expected relationship for a light curve with only white noise.

Fig. 5 shows an example of performing the RMS binning for an un-calibrated and calibrated light curve. The dashed lines show the expected relationship for a light curve with only white noise. The un-calibrated light curve deviates significantly from the expected relationship for white noise, indicating that it is dominated by systematic noise. The calibrated light curve, however, is much closer to the expected white noise relationship. As such, we can be confident that the comparison star used has successfully corrected the systematic trends. Hence, this method can be used to aid comparison star choice and to optimize the data reduction techniques used.

### 3.2 Pipeline

As discussed in Section 2.5, the optimum degree of binning cannot be determined theoretically, as the atmospheric conditions vary from night to night. Therefore, a pipeline was developed to determine the optimal number of frames that should be binned for a given data set.

Since the scientific target of interest will likely vary in magnitude, a test star should be used to determine the optimal temporal binning factor, $N_{\rm Opt}$, of the comparison star signal. Hence, in total, three stars are required. One must also determine whether the test star light curve and the comparison star light curve have systematic trends in common, which are likely common to the target.

A simulation was used to develop and test this pipeline. Simulated light curves with systematic trends, shot noise, read noise, and scintillation noise were produced for stars of different magnitudes.

The following pipeline was developed and tested using both simulated and observed star light curves. The steps below are used to determine the optimal temporal binning required to minimize the NSR of the calibrated target star:

(i) Perform the aperture photometry on the target star.

(ii) Select two other stars from the frame – a comparison star and a test star. These should be non-varying stars close to the target of interest, and ideally bright.

(iii) Perform the aperture photometry on the comparison star and test star.

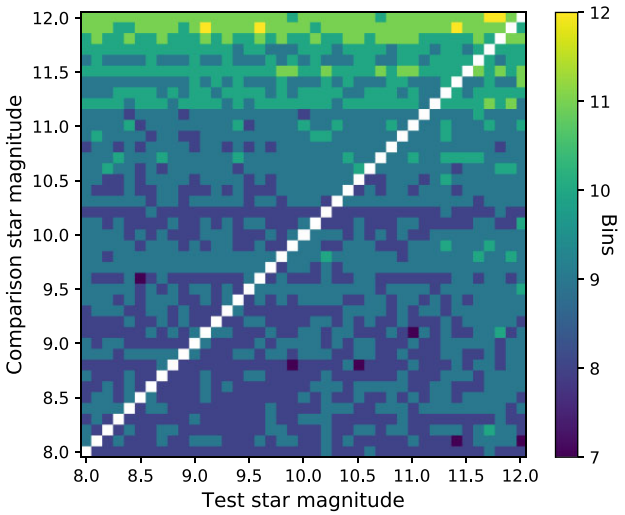


**Figure 6.** A matrix of the simulated optimized temporal binning factor, $N_{Opt}$, for a given comparison star magnitude as a function of the magnitude of the test star.

(iv) The cross spectrum of the light curves for the comparison and test stars are used to assess whether there are common systematic trends in the light curves that need correcting.

(v) Visually check the photometric light curves for any obvious high frequency trends – if there are periods of high frequency systematic trends, do not apply the temporal binning during these periods.

(vi) The selected comparison star is used to calibrate the test star with incremental binning i.e. start with no binning, then bin every two frames etc. The NSR of the calibrated test star is plotted as a function of the temporal binning applied to the comparison star light curve. This is used to find the binning factor $N_{Opt}$ that results in a minimum in the measured NSR of the calibrated test star light curve.

(vii) The RMS versus binning method described in Section 3.1 should be used on the un-calibrated and calibrated test star light curves to check that the use of the comparison star has reduced the systematic noise.

(viii) If the comparison star is deemed suitable in Step 7, then the target signal can now be calibrated using the comparison star light curve temporally binned by the optimal binning factor $N_{Opt}$ found in Step 6.

This pipeline could be combined with other techniques. For example, if multiple comparison stars are available, the stars signals could be averaged before applying the binning. In addition, the pipeline can be further optimized by allowing varying binning values in different parts of the light curve. For example, periods with higher frequency systematic trends could have less temporal binning than periods with lower frequency trends.

## 4 SIMULATIONS

For the available on-sky data, the minimum in the measured NSR is often very shallow (see Fig. 11). As such, it is hard to determine how the minimum location varies with the magnitude of the comparison star. Therefore, a simulation was used to produce light curves with second-order polynomial trends (such as Fig. 7) to produce more well defined $N_{Opt}$ (such as Fig. 8).

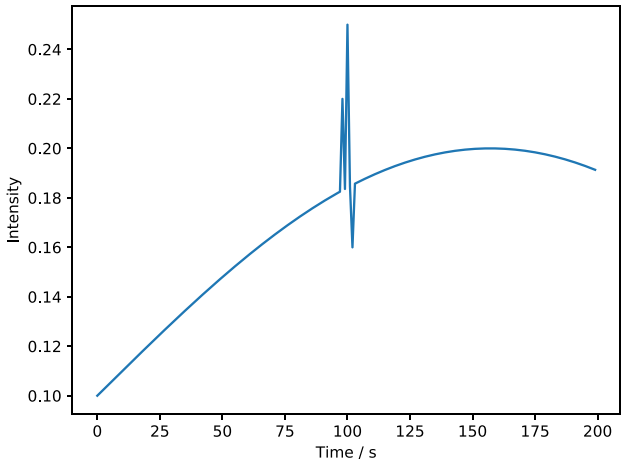


**Figure 7.** A simulated systematic trend with a low frequency second-order variation for a majority of the observing period and a high frequency trend between 98 and 102 s.

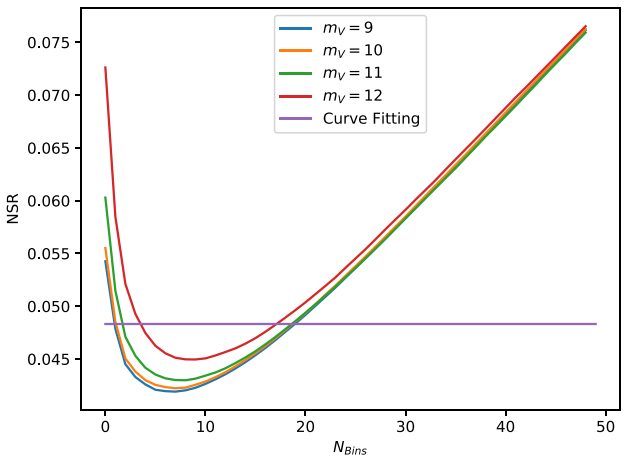


**Figure 8.** The NSR of the calibrated target light curve as a function of the temporal binning of the comparison star light curve for different magnitudes. The simulated comparison star light curve is temporally binned everywhere apart from the region of a rapid high frequency trend around 100 s. The purple line shows the measured NSR for the calibrated target star where a second-order polynomial fit has been used to correct the systematic trends.

Simulations were also used to investigate the impact of short periods of high frequency systematic noise e.g. due to cirrus clouds. This was done in simulation, since no data was collected in such conditions. All the data was either collected in good photometric conditions or during continuous poor conditions to the extent where the method could not be used at all.

### 4.1 Test star magnitude

Since the target of interest will likely have intrinsic variations, ideally another 'test' star should be used to determine the optimal temporal binning required. For a large telescope, the number of stars to choose from may be limited and therefore the test star may need to be relatively faint. In addition, the test star should be close to the target of interest to maximize the correlation for systematic trends. A simulation was used to check whether the magnitude of the test

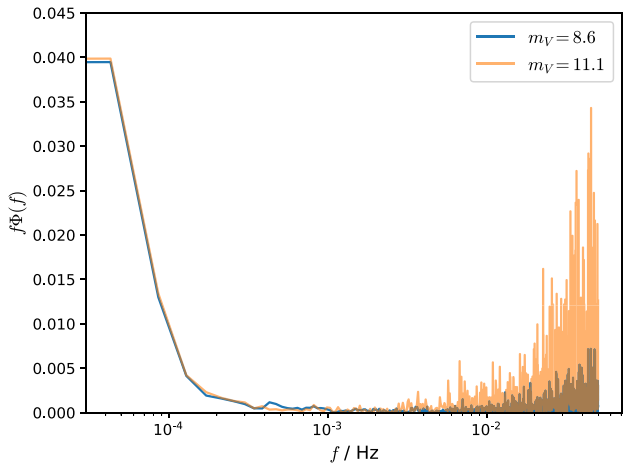


**Figure 9.** The power spectrum, $f\Phi(f)$, as a function of the frequency, $f$, for two stars of magnitude $m_V = 8.6$ and $m_V = 11.1$ observed with an NGTS telescope on 2021 February 18.

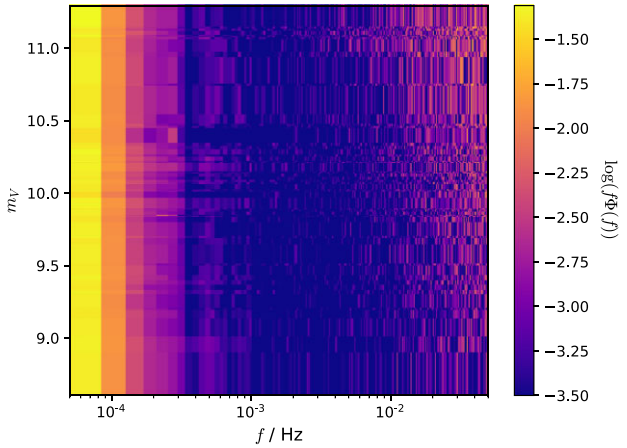


**Figure 10.** The power spectrum, $f\Phi(f)$, as a function of the star magnitude and log frequency, $f$, observed with an NGTS telescope on 2021 February 18.

star has a significant impact on determination of the optimal binning factor.

Light curves for a range of star magnitudes were produced, each with the same systematic trends, and random Poisson noise added according to the light level. Each star was used as a comparison star for each of the other light curves. The NSR of the calibrated test star against the temporal binning of the comparison star was measured and the binning that corresponds to the minimum NSR was recorded.

Fig. 6 shows the optimal binning required as a function of the comparison star magnitude and test star magnitude. The binning required does not appear to depend substantially on the test star magnitude used and depends primarily on the comparison star magnitude. Therefore, the test star does not need to have a similar magnitude to the target of interest. This is as expected, as the test star NSR is constant and therefore does not affect the position of the minimum. However, the brighter the test star magnitude, the better since the light curve should be dominated by the systematics trends that need to be corrected and not shot noise.

In reality, it is unlikely that the systematic trends in the light curves will be completely identical, as each star will likely have some localized systematic trends. Hence, a test star close to the target of interest on the detector should be selected to minimize the first-order atmospheric extinction and any other field dependent systematic trends.

### 4.2 High order (rapidly varying) trends

An important benefit of this method is that it can be optimized for each observation. For light curves with sudden rapid high order trends, for example due to intermittent cirrus cloud in otherwise photometric conditions, the comparison star can be temporally binned in the photometric periods and not binned (or less severely binned) in the periods that contain high order trends.

Fig. 7 shows an example systematic trend used in simulation. The systematic noise is primarily low in frequency, with a sudden high frequency trend at around 100 s. A magnitude $V = 8$ target star along with 4 comparison stars with $V = 9$, 10, 11, and 12 were simulated, all with this same systematic trends. Shot noise was added as appropriate for the star magnitude for a 1 s exposure time on the Pt5m telescope. The comparison stars were temporally binned everywhere except during the high frequency period at 98–102 s.

Fig. 8 shows the measured NSR of the calibrated light curve for each comparison star against the temporal binning of the comparison star. In addition, the NSR for the calibrated light curve using a second-order polynomial fit to correct the systematic trends is plotted. A minimum can be clearly seen for each comparison star. The steep increase in NSR for long integration times results from the shape of the low frequency systematic trend. In all cases, temporally binning the comparison star everywhere bar the high frequency period outperforms the use of a low order curve fitting algorithm and achieves a significantly reduced NSR at the minima. However, the curve fitting algorithm outperforms temporal binning of the comparison stars when more than 20 frames are temporally binned. This demonstrates the importance of selecting the optimum temporal binning for a given observation.

## 5 RESULTS

The pipeline described in Section 3.2 was tested with multiple on-sky data sets described in Section 5.1 and in simulation. In this section, we present the key results of testing this technique with on-sky data, including the application of the technique to two exoplanet transit light curves. We focus on bright targets of interest, since in these cases the calibrated signal is significantly limited by the magnitude of the comparison star. Whilst this technique is still useful in the case of a faint target, often a comparison star with a similar magnitude or brighter than the target will be within the FOV, and therefore the calibrated signal will still be dominated by the shot noise of the target signal.

### 5.1 Data sets

Here, we present results from the application of this pipeline to a variety of data sets. Details of the instrument used for each data set are given below.

#### *5.1.1 Pt5m*

Pt5m is a robotic 0.5-m telescope at the Roque de los Muchachos Observatory in La Palma, Spain (Hardy et al. 2015). This was used to collect the majority of the data used in this paper. This telescope

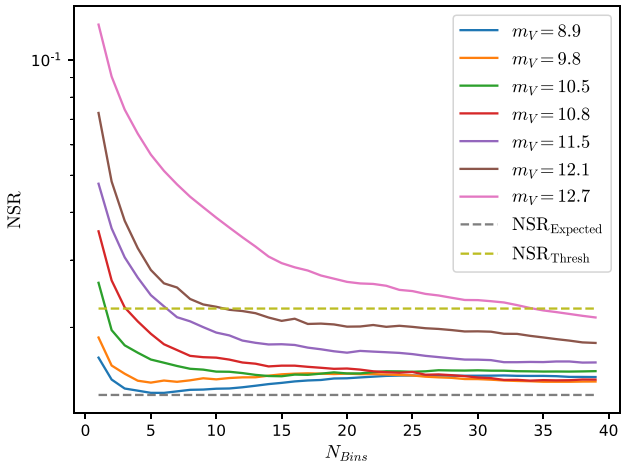


**Figure 11.** The NSR of the calibrated light curve as a function of the temporal binning of the comparison star. Only the comparison star is temporally binned. The threshold, $NSR_{Thresh}$, at which the addition of the random noise from the comparison star is outweighed by the correction of the systematic noise is also plotted along with the expected NSR which was estimated using the noise sources in the CCD equation (1) and the estimated scintillation noise for standard atmospheric conditions in La Palma.

provides imaging in standard photometric bands, with an FOV of 10.2 × 6.9 arcmin.

M36 (The Pinwheel Cluster, RA $05^h36^m16^s$ and Dec +34°08'36.5'), was chosen as a suitable target because it provides a large number of bright stars within the FOV. This target was observed on 15 nights between December 2020 and April 2021 using the Pt5m telescope. All observations were made in the *V* band with an exposure time of either 1 or 2 s. Each observation comprised of 100–300 frames with a cadence of ∼10 s.

#### *5.1.2 Wide-field camera data*

A wide field imager was used to acquire data from the Pt5m dome in La Palma in August and September 2016. The imager comprised a 70 mm *f*/1.8 lens coupled to a Moravian Instruments G3-11000 CCD camera, providing an FOV of 10 × 10 degrees.

A series of images were taken over several nights. The data were used to test the technique for the case of very bright stars. The NSR for the brightest stars from each night was measured and the effects of systematic errors on the NSR were investigated.

All observations were centred on RA $21^h05^m00^s$ and Dec + 29°00'00". Just over 48 h of data was collected over a 2 month period. Each night, an average of 600 frames were observed with a 10 s exposure and a cadence of 20 s. The telescope was slightly de-focused to avoid saturation. This data set was primarily used to investigate the binning of bright comparison stars to achieve the expected NSR reduction factor of $\sqrt{2}$.

#### *5.1.3 NGTS data*

Exoplanet transit data measured with the Next Generation Transit Survey (NGTS; Wheatley et al. 2017) was provided by Warwick University. NGTS is a wide-field robotic telescope facility designed to find and characterize transiting exoplanets at the ESO Paranal Observatory, Chile. NGTS is made up of twelve 20 cm robotic telescopes, each with an FOV of 8 square degrees. Each telescope uses a custom NGTS filter (520–890 nm).

The WASP-166b data was observed using a 10 s exposure time with NGTS on the 2021 February 18 (Doyle et al. 2022). The data from six of the 20-cm telescopes were averaged (Bryant et al. 2020). A total of 1384 images were collected by each telescope.

### 5.2 Power spectral density

This technique exploits the fact that the noise contribution from systematic noise is at low frequencies. On the other hand, if the systematic trends occur at high frequencies, then temporally binning the comparison star will reduce the correction achieved.

A key question therefore is whether stars of different magnitudes share the same low frequency trends i.e. whether there are any frequency-dependent effects in the light curve data reduction processing. Therefore, comparing the power spectrum of the target star light curve and comparison star light curve can give useful insight in to whether the comparison star selected is suitable and whether temporally binning the comparison star signal would be beneficial. NGTS data provided from 2021 February 18 was used to investigate how the power spectra from multiple stars in the field varies with magnitude. This data set was chosen due to its large FOV and hence large number of stars to compare.

Fig. 9 shows the power spectrum for a bright $m_V = 8.6$ and a fainter star of $m_V = 11.1$. We find that there are no significant difference in the power at low frequencies. As expected, for the fainter star, the higher frequencies have much more power due to increased shot noise. This clearly demonstrates the motivation of our proposed method and indicates that, for this observed data, the method is suitable.

Fig. 10 shows the power spectrum as a function of star magnitude and frequency for all the stars in the field. The power at the lowest frequencies does not change significantly with the star magnitude. At higher frequencies, there is an increase in power with star magnitude since, as expected, fainter stars have more shot noise.

Hence, we find that that fainter stars share the same low frequency trends as the bright stars and therefore, with temporal binning, substantially fainter stars can be used as comparison stars. However, the data is limited to a single observational set-up and does not have any stars fainter than a magnitude of $m_V = 11.3$. Therefore, similar studies from other telescopes and instruments would be useful in this context.

### 5.3 NSR

To investigate optimization of the temporal binning method, the NSR of the calibrated light curve was plotted as a function of the temporal binning for multiple comparison stars of different magnitudes.

The Pinwheel cluster data from the Pt5m telescope was used to test this method. A short exposure time of 1 s was used to ensure that the bright stars did not saturate the detector. The brightest star in the frame (of magnitude $V = 8.2$) was chosen as a target star, and fainter stars within the FOV were used as comparison stars.

Fig. 11 shows the NSR of the calibrated light curve as a function of the temporal binning factor, $N_{Bins}$, for a range of comparison stars with different magnitudes. The NSR decreases with increasing temporal binning. This is because the contribution of the photon and scintillation noise from the comparison star are reduced.

For the brightest comparison stars, where photon noise is less significant and the noise for the target is limited by scintillation, there is a slow increase in the NSR for long integration times such that a shallow minimum exists. This is because at long integration times

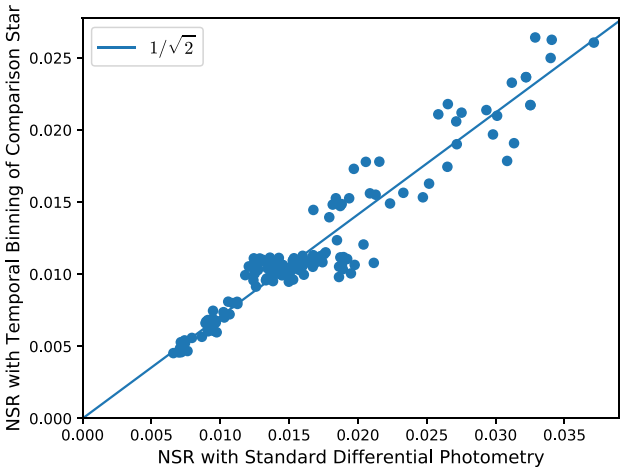


**Figure 12.** The NSR of the calibrated light curves with temporal binning of the comparison star versus the NSR of the calibrated light curve using standard (un-binned) differential photometry, for a range of stars dominated by scintillation noise. These results were produced using observations of the Pinwheel cluster on the Pt5m telescope and data using a wide-field camera in La Palma. Full details of these data sets are given in Section 5.1.

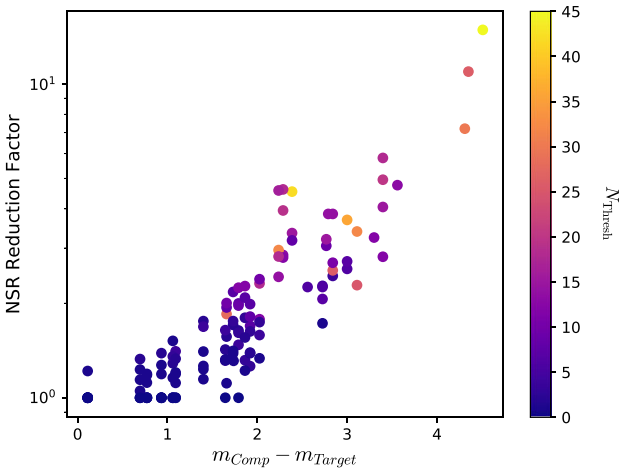


**Figure 13.** The reduction in the NSR versus the difference in magnitude between the comparison star ($m_{\mathrm{Comp}}$) and the target star ($m_{\mathrm{Target}}$). The temporal binning factor $N_{\mathrm{Thresh}}$ is given by the colour bar, where $N_{\mathrm{Thresh}}$ is the temporal binning required such that the addition of the random noise from the comparison star is outweighed by the correction of the systematic noise. This plot was produced using observations of the Pinwheel Cluster on the Pt5m telescope (see Section 5.1 for more details).

the atmospheric transparency variations and other low frequency systematic noise sources start to become significant. For the faintest comparison stars this feature is not seen as the photon noise contribution is far more significant.

In all cases temporally binning the comparison stars' data has reduced the NSR of the final light curve. In addition, there exists a binning factor at which using the comparison star does not add any additional noise to the calibrated light curve. The yellow dashed line represents the NSR of the raw target star light curve. At this NSR threshold, $NSR_{\mathrm{Thresh}}$, the addition of the random noise from the comparison star is outweighed by the correction of the systematic noise. The temporal binning factor of the comparison star signal that corresponds to this threshold is given by $N_{\mathrm{Thresh}}$. As binning reduces the noise contribution from the comparison star the NSR of the calibrated light curve should tend towards the expected NSR from the CCD equation and scintillation noise, given by the grey-dashed line. The RMS binning method in Section 3.1 was used to check that the comparison star has reduced the systematic noise.

### 5.4 Bright stars

Here, we test the case where both the target star and comparison star are bright. We expect that the random noise for both stars will be dominated by scintillation. Hence, we expect the NSR of the calibrated light curve will be reduced by a factor of $\sqrt{2}$ if we can employ the temporal binning of the comparison star light curve effectively. We employ two data sets from La Palma. The first data were collected in 2016 using the wide field camera described in Section 5.1.2. The second uses the Pt5m data of the Pinwheel Cluster described in Section 5.1.1. For each data set, we selected all of the bright comparison stars which were sufficiently bright to be expected to be dominated by scintillation. The brightest non-varying star from each night was selected as the target star and the remaining scintillation limited stars in the field were used as comparison stars.

Each target star light curve was calibrated using both the raw un-binned comparison star data and then with the comparison star data optimally binned using $N_{\mathrm{Opt}}$. Typically, we found $N_{\mathrm{Opt}} = 20$ although in many cases the minimum in the optimization curve was very shallow. In Fig. 12, we plot the NSR of the final light curve using optimized temporal binning against the NSR for standard (un-binned) differential photometry.

It was found that, on average, temporally binning the comparison star data reduced the NSR of the calibrated target star light curve by a factor of $1.41 \pm 0.06$, which agrees with the theoretical reduction of $\sqrt{2}$ within error. Hence, even when bright comparison stars are available, binning the comparison star is still beneficial.

**Table 1.** The comparison stars used, their magnitude in the *V* band and their distance from WASP-166b.

| Star | *V* | Distance (arcminutes) |
|---|---|---|
| TIC-413298649 | 9.45 | 44 |
| TIC-408307095 | 10.29 | 20 |
| TIC-408306501 | 11.31 | 45 |
| TIC-408306605 | 11.96 | 33 |

### 5.5 Faint stars

For faint stars, where the signal is photon noise limited, the NSR of the calibrated light curve can be reduced by a much larger factor, with the noise contribution from the comparison star reducing as $\sim \sqrt{N_{\mathrm{Bins}}}$. This was investigated using the observations of the Pinwheel Cluster from the Pt5m telescope.

The brightest star, with magnitude $V = 8.2$, was chosen as the target for each night of observations and the remaining stars in the field were used as comparison stars. For each comparison star, the temporal binning factor $N_{\mathrm{Thresh}}$, the point at which the correction of the systematic noise in the calibrated light curve outweighs the addition of random noise was recorded. In addition, the reduction in the NSR of the calibrated light curve at this point, was also recorded. The suitability of the comparison star was confirmed by visually checking that the NSR of the calibrated light curve was reduced to the threshold using the method described in Section 3.1.

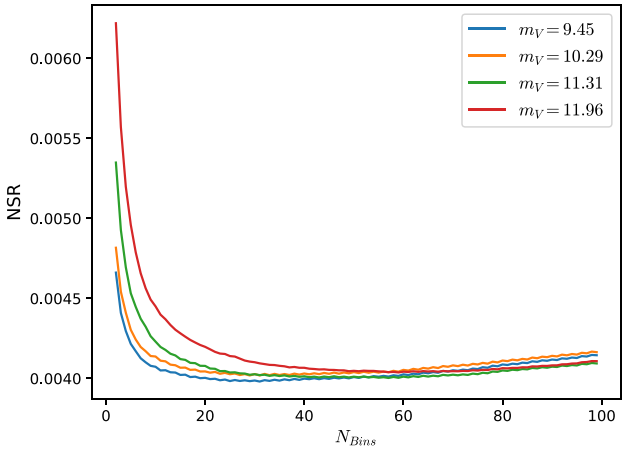


**Figure 14.** The NSR measured for the calibrated light curve for the test star, TIC-408354533, as a function of the temporal binning of the comparison star signal for four comparison stars outlined in table 1.

The results are shown in Fig. 13, which plots the factor by which the NSR of the calibrated light curve has been reduced by due to temporally binning the comparison star before performing the differential photometry. The colour bar shows the degree of temporal binning required, $N_{\rm Thresh}$, such that the correction of systematic noise with the use of the temporally binned comparison star outweighs the random noise contributions. In some cases, for bright comparison stars, this threshold is reached without any temporal binning.

The results show the expected relationship, where temporally binning bright comparison stars reduces the NSR by a factor $\sim \sqrt{2}$. Temporally binning fainter comparison stars reduces the NSR by a larger factor. The NSR is typically reduced by more than $\sim \sqrt{N}$. This indicates the presence of other random noise such as read-out noise and sky background light may be significant. In addition, larger temporal binning factors are required for the faint comparison stars which is to be expected from Fig. 3.

For the Pinwheel data, it was found that 44 per cent of the stars in the image field could be used to reduce the NSR of the calibrated light curve to $NSR_{\rm Thresh}$. In other words, by temporally binning the comparison star, we were able to reduce the contribution of random noise to a negligible level. Furthermore, we have shown that this is possible for comparison stars up to 4 mag fainter than the target star.

### 5.6 Transit analysis

#### *5.6.1 WASP-166b*

The method was tested on an exoplanet transit observation of WASP-166b, a hot Neptune around a magnitude $V = 9.35$ star, observed using a 10 s exposure time at a cadence of 13 s, with NGTS on the 2021 February 18 (Doyle et al. 2022). The data from six of the NGTS telescopes were averaged (Bryant et al. 2020).

A range of comparison stars were selected with magnitudes close to 0, 1, 2, and 3 fainter than WASP-166b. From these stars, a subset of comparison stars closest in position to the target star were selected in order to reduce first-order extinction effects. The details for the stars chosen are given in Table 1. The faintest star available has a magnitude of $V = 11.96$.

A test star, TIC-408354533, with magnitude $V = 10.29$ and a separation of 482 pixels (equivalent to 40'), from WASP-166b, was selected to find the binning required for each comparison star. Fig. 14 shows the measured NSR for the calibrated test star using the comparison stars in Table 1. For all curves a shallow minimum can be seen with a binning factor of around 30 for the two brighter stars, and 50 and 70, respectively, for the two fainter stars, resulting in the minimum NSR. As the temporal binning is increased beyond this point, the NSR also begins to slowly increase. This is due to the spectrum of the systematic noise, which has increased power at low frequencies.

Fig. 15 (a) shows the calibrated light curve using standard differential photometry and (b) shows the calibrated light curve where the comparison star light curves have been temporally binned with $N_{\rm Opt}$ frames. The calibrated light curve was temporally binned in 5-min intervals such that the transit can be clearly seen and in order to compare the average error between the bins in plot (a) and plot (b). The average error bar where the error bar for each time bin is calculated as $\sqrt{\frac{1}{\sum_i^n \sigma_i^{-2}}}$ where $\sigma_i$ is the standard error for telescope $i$, for each calibrated light curve is plotted in a black box in the bottom right-hand corner of (a) and (b). Comparing figs (a) and (b), it is clear that temporally binning the comparison stars has reduced the NSR.

We note that the scatter in the average light curve is slightly larger than expected from the individual error bars. This suggests that there is some residual correlated noise that is not being fully corrected via the comparison star measurements for this data. In some parts of the light curve there are clearly some low frequency trends which have not been fully corrected through the differential photometry. These are visible in the un-binned data as well, but are less obvious as the error bars are greater. In addition, the transit depth seems to vary slightly for the different comparison stars. We believe the main reason for this is due to the short shoulder measurements which have visible large systematic trends, especially at the egress. This is likely skewing the depth for the different comparison stars. Therefore this effect could be reduced with more data points prior and post to the transit.

Table 2 compares, for each comparison star, the average error bar of the noise in the calibrated light curve where standard differential photometry has been used and where the comparison star light curve has been temporally binned. Table 3 compares the average standard error of the calibrated transit light curves data points. Here, we see the effects of residual correlated noise such that the reduction factors are lower than in Table 2. For all the comparison stars, temporally binning by $N_{\rm Opt}$ frames has reduced the NSR of the calibrated transit light curve. In addition, with temporal binning, the use of a fainter comparison star performs nearly as well as the brightest comparison star (TIC-413298649).

A Markov chain Monte Carlo (MCMC) method was used to fit the transit photometry of WASP-166b using the `EMCEE` package (Foreman-Mackey et al. 2013) and the `batman` transit model package (Kreidberg 2015). We have used the parameters obtained by observations of WASP-166b given in Doyle et al. (2022) to perform the MCMC simulation. Twenty walkers with 10 000 steps per walker, with a burn in of 3000 steps were used. Only the mid-transit time, $T_0$, the planet radius, $R_{\rm p}$, and the limb-darkening coefficients were varied, with all remaining parameters fixed. During the MCMC analysis, a linear out-of-transit model with time is fitted to each light curve simultaneously with the transit model.

Table 4 shows the results for the fitted $T_0$ for the calibrated light curve using each comparison star with standard differential photometry and with temporal binning of the comparison star light curve. In all cases temporally binning the comparison star signal results in a higher precision. Doyle et al. (2022) found $T_0 = 2459264.729337 \pm 0.000633$. All of our transit times are consistent with this result and with the *TESS* prediction within $3\sigma$.

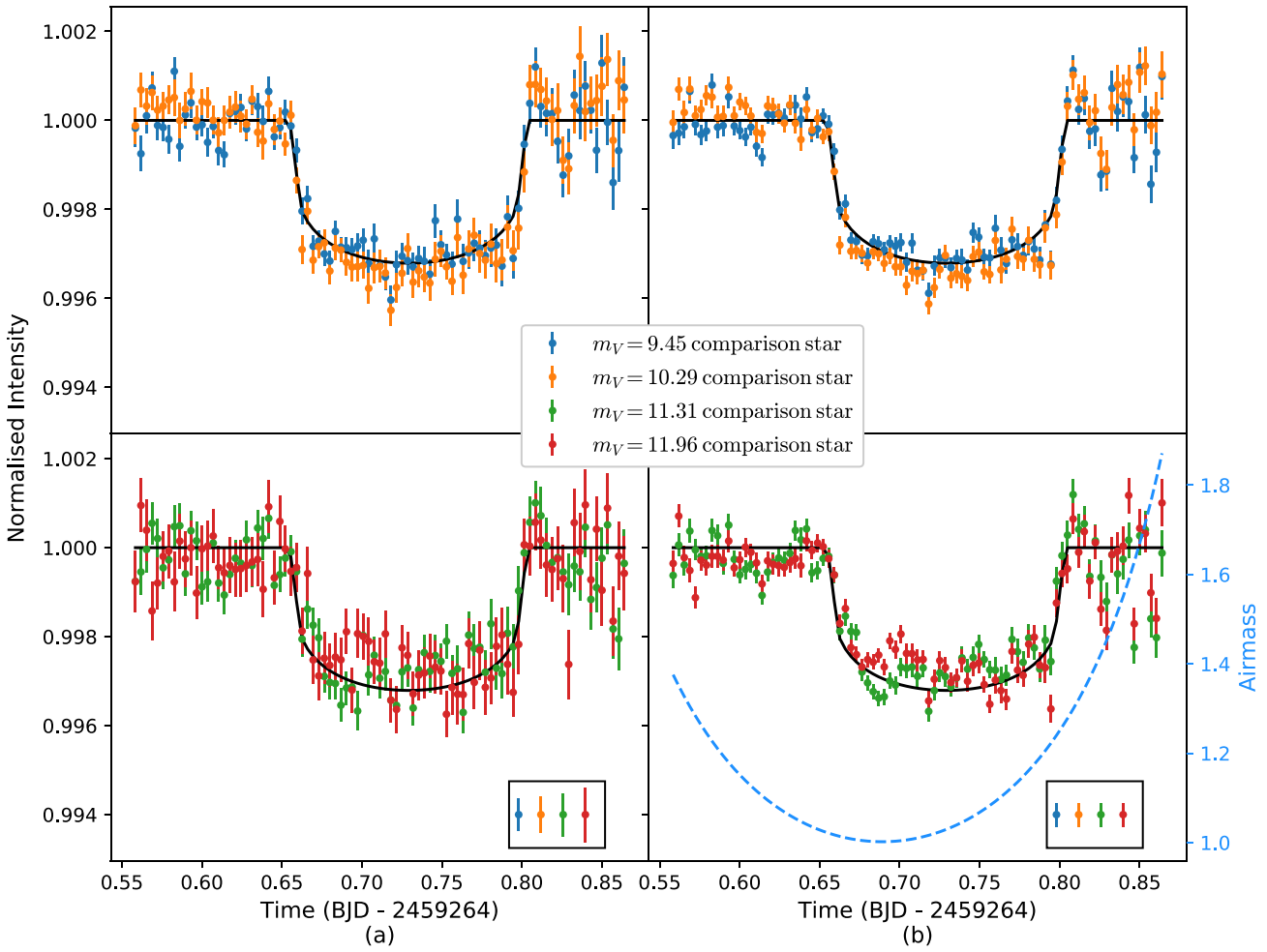


**Figure 15.** The transit light curve for WASP-166b observed on 2021 February 18 with 6 NGTS telescopes. The left-hand plots (a) show the calibrated light curve using standard differential photometry and the right-hand plots (b) show the calibrated light curve where the comparison star light curves have been temporally binned by $N_{\mathrm{Opt}}$ frames. The calibrated light curve was then temporally binned in 5-min intervals such that the transit can be clearly seen and in order to compare the average error between the bins in plot (a) and plot (b). The bottom right-hand plot also has the airmass plotted as the blue dashed line. The average weighted standard error calculated for each time bin as $\sqrt{\frac{1}{\sum_i^n \sigma_i^{-2}}}$ where $\sigma_i$ is the standard error of telescope $i$, is indicated by the error bars in the bottom right-hand corner of each subplot. The theoretical transit light curve using the fitted parameters of TESS data presented in Doyle et al. (2022) is also plotted.

**Table 2.** The average error bar for the calibrated transit light curve of WASP-166b using standard differential photometry compared with the error bar with temporal binning of the comparison star light curve.

| Star | Standard differential photometry $\sigma$ | Temporal binning $\sigma$ | Reduction factor |
|---|---|---|---|
| TIC-413298649 | $3.7 \times 10^{-4}$ | $2.6 \times 10^{-4}$ | 1.40 |
| TIC-408307095 | $4.0 \times 10^{-4}$ | $2.6 \times 10^{-4}$ | 1.53 |
| TIC-408306501 | $4.8 \times 10^{-4}$ | $2.6 \times 10^{-4}$ | 1.84 |
| TIC-408306605 | $6.1 \times 10^{-4}$ | $2.6 \times 10^{-4}$ | 2.32 |

### 5.6.2 *Qatar 1b*

A transit of Qatar-1b, a magnitude $V = 12.84$ star with a transit depth of 0.02 mag, was observed using a 20 s exposure time, with a cadence of 31 s, on the Pt5m telescope on the 2022 June 11. The FOV (10.2 × 6.9 arcmin) is much more limited for this telescope compared to NGTS. As such, there were far fewer comparison stars to choose from than in the previous example.

**Table 3.** The average scatter for the calibrated transit light curve of WASP-166b using standard differential photometry compared with the average scatter with temporal binning of the comparison star light curve. Here, we see the effects of residual correlated noise such that the reduction factors are lower than in Table 2. However, the overall noise is still reduced in all cases.

| Star | Standard differential photometry $\sigma$ | Temporal binning $\sigma$ | Reduction factor |
|---|---|---|---|
| TIC-413298649 | $3.2 \times 10^{-4}$ | $2.9 \times 10^{-4}$ | 1.14 |
| TIC-408307095 | $3.7 \times 10^{-4}$ | $3.2 \times 10^{-4}$ | 1.17 |
| TIC-408306501 | $4.4 \times 10^{-4}$ | $3.2 \times 10^{-4}$ | 1.43 |
| TIC-408306605 | $5.7 \times 10^{-4}$ | $3.8 \times 10^{-4}$ | 1.62 |

A star of magnitude $V = 13.5$ was used to perform the differential photometry. A test star of magnitude $V = 12.98$ was selected from the field to determine the temporal binning required. Fig. 16 shows the NSR of the calibrated light curve for the test star against the temporal binning of the comparison star. In this example, no clear minimum in

**Table 4.** The MCMC fitted mid-transit time, $T_0$, for the calibrated transit light curve of WASP-166b using standard differential photometry compared with the temporal binning of the comparison star light curve.

| Star | Standard differential photometry | Temporal binning |
|---|---|---|
| TIC-413298649 | 2459264.73025 ± 0.00060 | 2459264.73027 ± 0.00043 |
| TIC-408307095 | 2459264.73002 ± 0.00051 | 2459264.72988 ± 0.00037 |
| TIC-408307086 | 2459264.72886 ± 0.00105 | 2459264.72862 ± 0.00059 |
| TIC-413298350 | 2459264.73029 ± 0.00119 | 2459264.73073 ± 0.00064 |

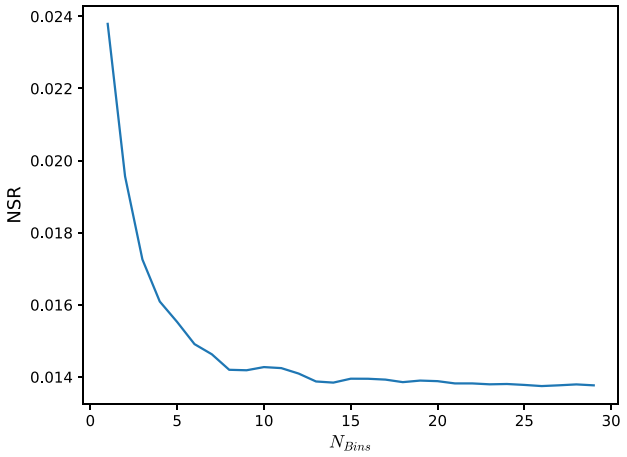


**Figure 16.** The NSR of the calibrated light curve for the test star as a function of the temporal binning factor of the comparison star observed on 2022 June 11 using the Pt5m telescope.

the NSR is visible. This is because the systematic noise is dominated by a linear trend and therefore severe binning still accurately corrects the systematic noise.

Fig. 17 shows the calibrated light curve using standard differential photometry and the case where the comparison star has been temporally binned by 25 frames. The NSR of the calibrated light curve using standard differential photometry is $2.1 \times 10^{-2}$. Temporally binning the comparison star has reduced the NSR of the calibrated transit by a factor of 2, to an NSR of $1.0 \times 10^{-2}$. The NSR of the un-calibrated Qatar-1b transit data was $1.3 \times 10^{-2}$. Thus, we have shown that a fainter comparison star can be used without adding any noise to the final light curve at this cadence.

## 6 DISCUSSION

Choosing a suitable comparison star is of great importance for high-precision photometry since any residual systematics in the differential photometry will add linearly. In addition, the random photon noise and scintillation noise of the star of interest and the comparison star will add in quadrature. The data reduction technique described here significantly reduces the NSR for differential photometry by taking advantage of the fact that power in systematic trends is often at low frequencies compared to the cadence of the light curve. Hence, a minimum exists in the total noise of a light curve as a function of the integration time and cadence. Therefore, the total NSR of the calibrated light curve can be minimized by optimizing the temporal binning.

One of the main advantages of this binning method is that it allows much fainter comparison stars to be used. This is especially beneficial for less dense fields where there are few comparison stars available

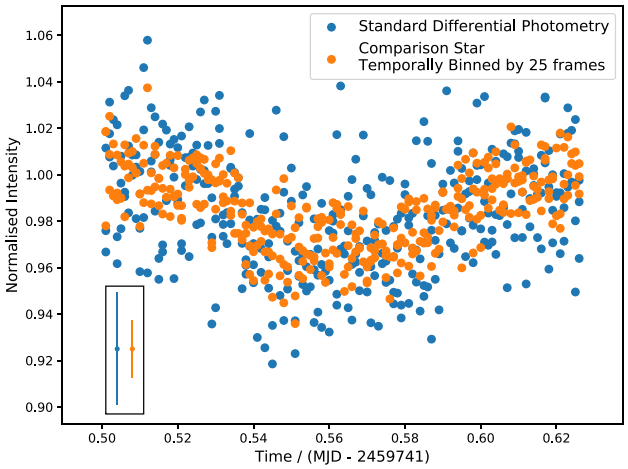


**Figure 17.** The calibrated transit light curve of Qatar-1b observed on 2022 June 11 on the Pt5m telescope using standard differential photometry in blue and where the comparison star has been temporally binned by 25 frames in orange. The standard deviation measured at the wings of the transit for each method is given in the bottom left-hand corner.

and for large telescopes where the FOV is small. In this case there are often few comparison stars to choose from and therefore calibration methods, such as averaging multiple comparison stars, are limited. This technique is also beneficial for small telescopes where, whilst there are more comparison stars in the FOV to choose from, the scintillation noise is more significant, scaling as $D^{-4/3}$, where $D$ is the aperture size.

This technique can also be implemented in addition to other data reduction methods such as the use of multiple comparison stars and the defocussing technique (Tregloan-Reed & Southworth 2013) and diffuser technique (Stefansson et al. 2017), thus resulting in even lower NSRs.

It should be noted that this method is only beneficial for observations that are taken in good photometric conditions. The systematic trends in the data must be at low frequencies for the binning of the comparison star to be beneficial. For observations with high frequency systematic noise the comparison star can no longer be binned, as the moving average would smooth out these trends and thus no longer accurately correct the systematic noise for the target star.

For observations that have occasional periods of sudden high frequency trends, binning could still be beneficial. The comparison star data would be temporally binned everywhere except for periods of rapid high frequency trends. As such, the calibrated light curve would still have these periods of high frequency trends corrected by the comparison star. The NSR of the light curve would be improved everywhere except for the high frequency periods where the NSR would be equivalent to the use of standard differential photometry. This flexibility with where the binning is applied is another advantage to this method over the use of low order curve fitting algorithms, as any high order trends can still be corrected.

In addition, we have demonstrated that this technique works for a range of cadence values up to 30 s. We expect this method to work for cadences of the order of tens of seconds in cases dominated by shot noise and scintillation noise. In addition, we have demonstrated the technique on two exoplanet light curves and have shown that temporal binning of the comparison stars reduces the NSR of the calibrated transit light curve as shown in Tables 2 and 3. Hence, this data reduction technique is ideal for ground-based follow-

up observations of exoplanets around bright stars such as targets found by *TESS* (Villanueva, Dragomir & Gaudi 2019), SuperWASP (Pollacco et al. 2006), MASCARA (Lesage et al. 2014), and NGTS (Wheatley et al. 2017).

Information about telescope sites can also be gained from this technique. Measuring the minima in the NSR versus time plots (such as the minima in Fig. 14) for a range of standard stars over multiple nights could provide details of the power spectrum of the atmospheric transparency fluctuations of the site and the observed scintillation noise. Therefore, these could be used to perform a statistical survey of seasonal and cyclical variations in photometric quality.

Further research investigating this technique in multiple wavebands is needed. Simultaneous observations in multiple wavebands could be used to investigate how the power spectrum of the atmospheric transparency variations vary with wavelength and therefore the viability of this method in different wavebands.

## 7 CONCLUSIONS

Differential photometry is critical to correct systematic trends in high-precision ground-based photometry. However, the NSR of the calibrated light curve is then limited by the random intensity fluctuations of the target and comparison star as the shot noise and scintillation noise of the raw light curves add in quadrature.

We propose that, since the time-scale of the systematic variations is much longer than the cadence, often the comparison star can be temporally binned before performing the differential photometry, therefore reducing the NSR of the calibrated light curve. The temporal binning of the comparison star is optimized by finding the integration time that results in the minimum NSR for the calibration of a non-varying test star.

We have shown that, for a bright, scintillation limited target and comparison star, temporally binning the comparison star can reduce the NSR of the calibrated light curve by a factor of $\sqrt{2}$. For a fainter comparison star, limited by photon noise, the NSR is reduced by a larger factor. This allows the use of much fainter comparison stars. In our observations, we have found that comparison stars of up to four magnitudes fainter than the target star can be used.

We have described a data pipeline to perform this technique and to optimize the temporal binning used. An example transit light curve of WASP-166b observed using six of the NGTS telescopes has been presented. Light curves using four comparison stars of different magnitude were produced. In all cases temporally binning the comparison star before doing the differential photometry reduced the NSR of the calibrated transit light curve.

## ACKNOWLEDGEMENTS

This work was supported by the Science and Technology Facilities Council [ST/N50404X/1] and [ST/T506047/1]. The authors would like to thank Warwick University and the NGTS consortium for access to the WASP-166b NGTS data, with special thanks to Edward Bryant.

This research made use of PYTHON including NUMPY and SCIPY (van der Walt, Colbert & Varoquaux 2011), MATPLOTLIB (Hunter 2007), ASTROPY, a community-developed core PYTHON package for Astronomy (The Astropy Collaboration 2013) the Python AO utility library `AOtools` (Townson et al. 2019).

## DATA AVAILABILITY

Please contact Kathryn Hartley for data availability.

## REFERENCES

Boyd D., 2007, SASS, 26, 119
Bryant E. M. et al., 2020, MNRAS, 494, 5872
Doyle L. et al., 2022, MNRAS, 516, 298
Dravins D., Lindegren L., Mezey E., Young A. T., 1997, Publ. Astron. Soc. Pac., 109, 173
Fohring D., Dhillon V. S., Madhusudhan N., Marsh T.R., Copperwheat C.M., Littlefair S.P., Wilson R.W., 2013, MNRAS, 435, 2268
Foreman-Mackey D., Hogg D. W., Lang D., Goodman J., 2013, Publ. Astron. Soc. Pac., 125, 306
Föhring D., Wilson R., Osborn J., Dhillon V., 2015, J. Phys. Conf. Ser., 595, 012010
Giannini E. et al., 2017, A&A, 597, A49
Hardy L. K., Butterley T., Dhillon V. S., Littlefair S. P., Wilson R. W., 2015, MNRAS, 454, 4316
Hartley K. E., Farley O. J. D., Townson M. J., Osborn J., Wilson R. W., 2023, MNRAS, 520, 4134
Hill F. et al., 1994, Sol. Phys., 152, 321
Howell S. B., 1989, Publ. Astron. Soc. Pac., 101, 616
Howell S. B., 1992, ASPCS, 23, 105
Howell S. B., 2006, Handbook of CCD Astronomy, 2 edn. Cambridge Observing Handbooks for Research Astronomers, Cambridge University Press, Cambridge
Howell S. B., Jacoby G. H., 1986, Publ. Astron. Soc. Pac., 98, 802
Hunter J. D., 2007, Comput. Sci. Eng., 9, 90
Koppelman M., 2005, SASS, 24, 107
Kornilov V., 2012, MNRAS, 426, 647
Kreidberg L., 2015, Publ. Astron. Soc. Pac., 127, 1161
Lesage A. L., Spronck J. F. P., Stuik R., Bettonvil F., Pollaco D., Snellen I. A. G., 2014, in Stepp L. M., Gilmozzi R., Hall H. J.eds, Proc. SPIE Conf. Ser. Vol. 9145, Ground-based and Airborne Telescopes V. SPIE, Bellingham, p. 914514
Mann A. W., Gaidos E., Aldering G., 2011, Publ. Astron. Soc. Pac., 123, 1273
Osborn J., 2014, MNRAS, 446, 1305
Petigura E. A., Marcy G. W., 2012, Publ. Astron. Soc. Pac., 124, 1073
Pluzhnik E. A., 2005, A&A, 431, 587
Poddaný S., Brát L., Pejcha O., 2010, New Astron., 15, 297
Pollacco D. L. et al., 2006, Publ. Astron. Soc. Pac., 118, 1407
Pont F., Zucker S., Queloz D., 2006, MNRAS, 373, 231
Sasiela R. J., 2012, Electromagnetic Wave Propagation in Turbulence: Evaluation and Application of Mellin Transforms, Vol 18 (Springer Series on Wave Phenomena), Springer, Berlin
Southworth J. et al., 2009, MNRAS, 396, 1023
Stebbins J., 1910, ApJ, 32
Stefansson G. et al., 2017, ApJ, 848, 9
The Astropy Collaboration, 2013, A&A, 558, A33
Townson M. J., Farley O. J. D., de Xivry G. O., Osborn J., Reeves A. P., 2019, Opt. Express, 27, 31316
Tregloan-Reed J., Southworth J., 2013, MNRAS, 431, 966
Villanueva Steven J., Dragomir D., Gaudi B. S., 2019, AJ, 157, 84
Wheatley P. J. et al., 2017, MNRAS, 475, 4476
Young A. T. et al., 1991, Publ. Astron. Soc. Pac., 103, 221
Zou H. et al., 2010, AJ, 140, 602
van der Walt S., Colbert S. C., Varoquaux G., 2011, Comput. Sci. Eng., 13, 22

This paper has been typeset from a TEX/LATEX file prepared by the author.